Additive Manufacturing of Thermally Enhanced Lightweight Concrete Wall Elements with Closed Cellular Structures

Gido Dielemans[1*], David Briels[2], Fabian Jaugstetter[1], Klaudius Henke[3], Kathrin Dörfler[1]

*   Corresponding author

1   TT Professorship Digital Fabrication, Department of Architecture, Technical University of Munich, Munich, Germany, gido.dielemans@tum.de

2   Chair of Building Technology and Climate Responsive Design, Department of Architecture, Technical University of Munich, Munich, Germany

3   Chair of Timber Structures and Building Construction, Department of Civil, Geo and Environmental Engineering, Technical University of Munich, Munich, Germany

Abstract

Building envelopes incorporate a multitude of functions, such as structure, room enclosure, insulation, and aesthetic appeal, typically resulting in multi-material layered constructions. With the technology of additive manufacturing, geometrical freedom can instead be utilised to integrate functional requirements into mono-material building components. In this research, the additive manufacturing method of lightweight concrete extrusion and its potential for thermal performance via geometric customisation is explored. It investigates whether the insulating performance of wall components can be increased through the creation of closed cellular structures, and further, whether these performance features can be functionally graded by locally adapting the geometric properties. A design tool for closed-cell wall geometries is created, which integrates lightweight concrete extrusion related fabrication constraints and takes into account thermal and structural performance considerations. Through the simulation of heat transfer, generated wall geometries are analysed for their thermal performance. By calculating the layer cycle times and determining the overhang during extrusion, the structural capacity during printing is validated. Finally, experimental manufacturing of 1:1 scale architectural prototypes is executed to test the feasibility of the concept.

Keywords

Additive manufacturing, lightweight concrete extrusion, computational design, thermal performance, functionally graded materials

1 INTRODUCTION

Computer-aided design has enabled architects and engineers to construct a formal language with unprecedented geometric complexity and attention to detail. Additive Manufacturing (AM) methods in construction such as 3D Concrete Printing (3DCP) are the response to this paradigm shift as a method with which complex designs can be materialised. In extrusion-based 3DCP, fresh concrete is deposited layer by layer, shaping concrete without formwork and placing the material only where desired. In view of the large ecological footprint of the construction sector, recent research has increasingly investigated how this new technology redefines architectural design-to-realisation strategies and enables the production of material-effective structures through structural optimisation and geometric customisation (Agustí-Juan & Habert, 2017). While research has made remarkable technological advances, the construction of fully functional spaces with AM technology applied to building envelopes requires architects and engineers to also consider climatic performance features. At this time, constructions produced utilising 3DCP are still rather modest in terms of integrating aspects of human comfort and ensuring a suitable indoor climate when compared to most traditional fabrication alternatives.

In this paper, building components are integrated with climatic performance functions through exploration of geometric freedom provided by 3DCP. It investigates whether the geometric properties of closed cellular geometries of lightweight concrete can increase the insulating performance of mono-material wall components (see Fig. 1), and further, whether these performance features can be functionally graded by locally adapting the geometric properties. It then investigates whether such mono-material building components can present a viable alternative to conventional layered multi-material constructions for fulfilling thermal functions. The experimental methodology of this research enabled the realisation of two prototypes, which provided essential insights into the feasibility of the concept.

FIG. 1 Close-up of a concrete cellular structure manufactured using extrusion-based 3DCP (Jaugstetter, 2020).

2   STATE OF THE ART

Recent research has brought forward a few approaches in achieving increased climatic performance with building components manufactured using AM methods. Closely related to conventional layered construction, one method applies insulating material to the outside of an additively manufactured structural concrete element. This was shown in the Office of the Future in Dubai (Dubai Future Foundation, n.d.) and the structural wall of the multi-storey house at Kamp C in Westerlo (Van Der Putten et al., 2020). The filling of cavities in the 3DCP structural system with insulation is a second approach, which has been applied to the case study of the Nyborg Studio (Bos, Wolfs, Ahmed, & Salet, 2019), and the insulated wall of the multi-storey house at Kamp C in Westerlo (Van Der Putten et al., 2020). A reverse approach using additively manufactured geometries of insulating material as lost formwork for the casting of concrete has been researched with the Digital Construction Platform by the Mediated Matter Group at MIT (Keating, Leland, Cai, & Oxman, 2017). Additionally, a house dubbed *Yhnova* was constructed using a similar technique called Batiprint3D as part of the Nantes Digital Week (Furet, Poullain, & Garnier, 2019). Besides the addition of insulation materials, other approaches are being developed that alter the material composition of concrete with the aim of increasing thermal insulation capacity, and reducing component weight and material usage. The research direction of foamed concrete for AM has most recently been explored at the TU Dresden (Markin, Ivanova, Fataei, Reißig, & Mechtcherine, 2020) and the Polytechnic of Turin (Falliano et al., 2020), where reduced material density was achieved by creating regular air cavities in the concrete while material strength and rheological properties are maintained. Another approach of material research for AM with thermal insulation in mind is through the use of lightweight aggregates in the concrete mixture (Henke, Talke, & Matthäus, 2020).

While research has proven the thermal capacity of building components to increase by adding insulating materials or by altering the material composition, one potential method for functional enhancement is the geometric manipulation of a mono-material building component. This can be done through an optimisation process, iteratively improving structural and thermal performances by altering the cross-sectional shape of the building component (Vantyghem, Steeman, De Corte, & Boel, 2020). More elaborate graded materials can be created by enclosing air in the geometry of the object, inspired by natural occurring meso-materials like wood, coral and cancellous bone (Vantyghem, Steeman, De Corte, & Boel , 2017). Due to the internal geometry of the structure, these materials benefit from high strength capacity, light weight, improved thermal conductivity, and electrical resistance. Applying this geometrical philosophy to the macro scale has the potential to improve thermal and structural characteristics, but results in complex geometries that can only be created with advanced manufacturing processes. With the potential for complex geometries in 3DCP, this research further explores geometrical design with the aim to achieve higher thermal performance.

3   METHODOLOGY

In order to fundamentally address the topic of thermal improvement of building components with concrete AM, this research is carried out at the interface between architecture, climate responsive design, and materials science. By creating a computational design tool, possible shapes of closed-cell geometries are investigated for their potential as thermal insulator, enabled by 3DCP of lightweight concrete (Henke et al. 2020). In continuation, the modelling of a continuous extrusion print path of the cellular geometry according to associated manufacturing constraints is explored.

The geometric results are then thermally evaluated in simulation, and experimentally validated for production feasibility through prototype manufacturing.

3.1   DESIGN PRINCIPLE

Cellular structures can be divided into open-cell and closed-cell typologies. Open-cell structures in concrete extrusion practice are often applied for stabilisation and material reduction; additionally, these cells can be filled with insulating material. While open-cell typologies such as honeycomb or simple zigzag patterns are the most common internal designs, AM technology also allows for three-dimensional internal design, where volumes are enclosed in the structure.

To tessellate internal space entirely, only five three-dimensional geometric solids are suitable to be arrayed: the cube, prism, rhombic dodecahedron, elongated dodecahedron, and truncated octahedron (see Fig. 2). While all these shapes can tessellate space, a high volume to a low surface area is advantageous for limiting heat losses through conduction. With its 14 faces, the truncated octahedron is the shape that adapts most closely to the ideal ratio of a sphere, and was thus chosen as the basis for geometrically modelling the closed cell structures of this research.
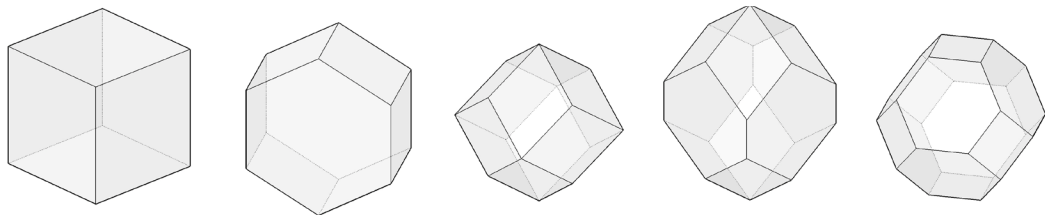
FIG. 2   The five main space-filling polyhedra. From left to right: Cube, Prism, Rhombic Dodecahedron, Elongated Dodecahedron, and the chosen Truncated Octahedron (Jaugstetter, 2020).

In this research enclosed air volumes are constructed using support-free 3DCP, applied at the building scale. Creating closed cells, with an encapsulated volume that holds air, is not possible in all AM technologies. Particle bed solutions, for instance, would result in the particulates being trapped inside the structure (Weger et al., 2020). The unique thermal properties of closed-cell typologies are evidenced by closed-cell foams, which have the lowest thermal conductivity of any conventional non-vacuum insulation (Gibson & Ashby, 2014).

3.2   DESIGN TOOL

To design and evaluate closed-cell geometries that integrate the production constraints of 3DCP, a design tool was created in Rhino (McNeel & Associates, n.d.) and Grasshopper, supplemented with specially developed Python scripts (see Fig. 3). A wall element was chosen as a use-case to examine the enhancement strategy. Two guide surfaces are defined to shape the outer boundaries of the element, defining parameters such as width, height, and length of the component. An attractor point can be placed in the wall element to vary the density of the cells inside the wall, for example, to locally increase the loadbearing behaviour of the wall, or satisfy design-related decisions. The cell size can be changed in width, depth, and height to affect structural and thermal performance, for which the user is guided by a performance feedback.

The context of this feedback is constructed from process parameters in the design tool, like layer height, filament width, ideal layer cycle time, and maximum overhangs.
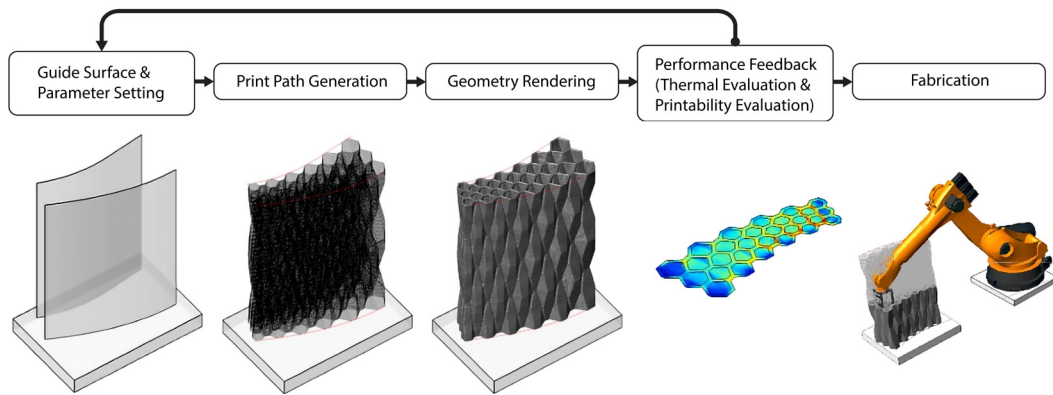

FIG. 3 Overview of the proposed parametric design tool, which integrates the modelling of the closed-cell geometry and the associated print path according to the given boundary surfaces, the rendering of the resulting geometry, and the evaluation possibilities of defined performance criteria for the generated geometry (Jaugstetter, 2020).
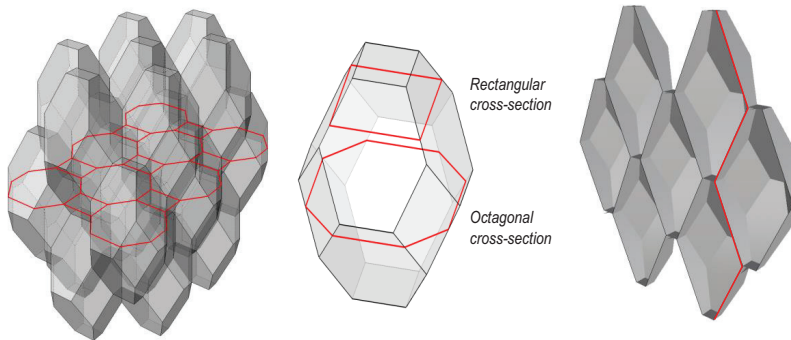

FIG. 4 Truncated octahedron geometry with rectangular and octagonal path slices (Jaugstetter, 2020)

The chosen cell geometry of a truncated octahedron has two cross-section types within the slicing procedure, an octagonal and a rectangular section (see Fig. 4). Over the height of the cell the path length follows a periodic trend, with the shortest rectangular paths at either end.

To manufacture an array of these cells, a print path is modelled as a sequence of incremental vectors describing the geometry of half a cell (see Fig. 5), which is inspired by turtle graphics (Goldman, Schaefer, & Ju 2004). To evaluate the change of cross-sectional geometry and print path length, a function has been defined describing the behaviour:

$$f(x) = \pm \frac{a}{\pi} \sin^{-1}\left(\cos\left(\pi \frac{x-p}{p}\right)\right) + \frac{a}{2} \qquad (1)$$

The first derivative of the previous function defines the point at which sectional geometry changes:

$$f'(x) = \frac{a}{\pi}\sin^{-1}\left(\cos\left(\pi\frac{x-2p}{2p}\right)\right) + \frac{a}{2} \qquad (2)$$

To make this approach valid for freeform elements, the cellular structure needs to adapt by reorientating the sequence and varying the width and depth of the cell. This adaptation is done by evaluating points on the centreline of the structure, where the angle, tangent, and normal of the point on the curve represent the reorientation angle, width, and depth respectively (Fig. 6). The height of the cell is remained fixed in accordance with process parameters, like layer height and maximum overhangs.
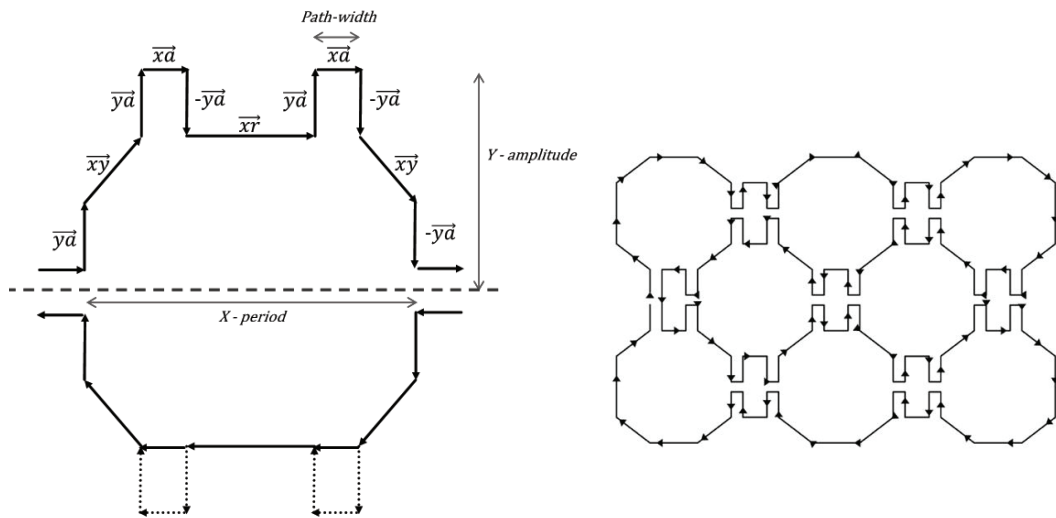
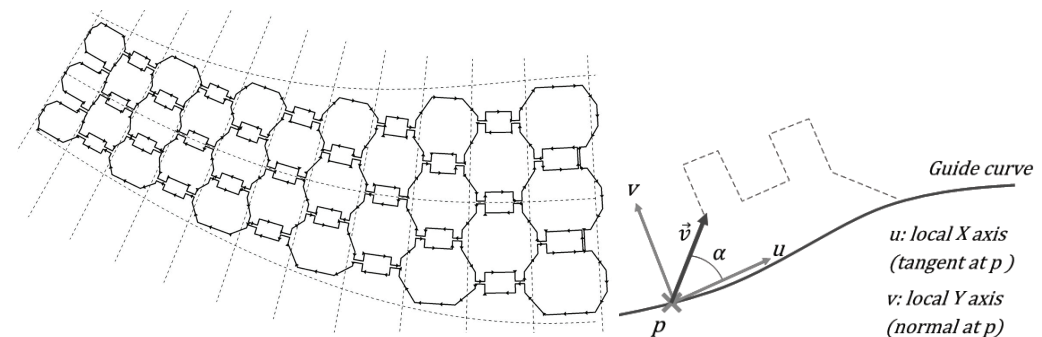FIG. 5 Print path geometry, built from vector sequencing (Jaugstetter, 2020)

FIG. 6 Vector sequence according to a guide curve: $\vec{v}$: vector of vector sequence, α : reference angle, p : reference point (left), and applying the system to two boundary surfaces (right) (Jaugstetter, 2020)

3.3 PERFORMANCE FEEDBACK

3.3.1 Thermal Performance

The thermal conductivity of cellular structures comprises conduction through the solid and gas as well as convection and radiation within the cells (Gibson & Ashby, 2014). Air is an insulator with low thermal conductivity when in a rested state; in a moving state, however, heat transfer is accelerated as a result of convection (Bankvall, 1972). Convection can be reduced by encapsulating air in cells, limiting buoyancy-driven natural convection, with decreasing sizes of encapsulating volumes having reduced natural convection (Gibson & Ashby, 2014). For closed-cell foams it was found that convection can be neglected at a maximum cell size of 10 mm (Gibson & Ashby, 2014). Opposite to convection, conduction increases with decreasing air layer thickness. Considering the combined heat transfer, a study by Bekkouche et al. (2013) described an ideal air layer thickness of 40 to 60 mm for a cavity wall under given assumptions (see Fig. 7).
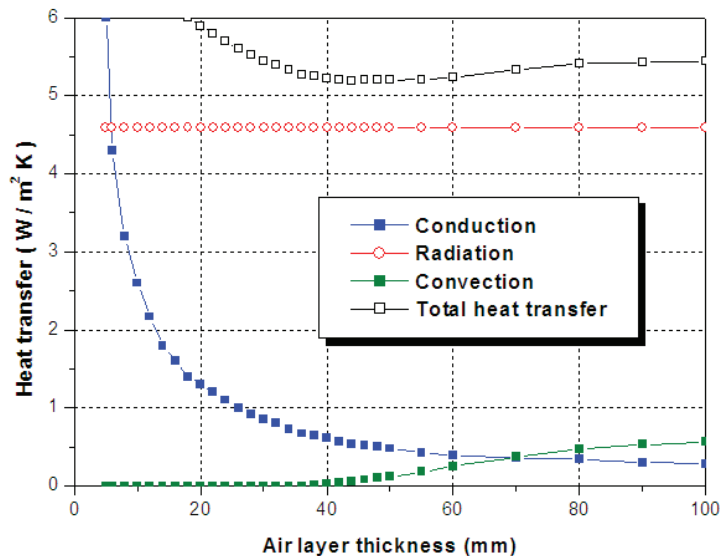

FIG. 7 Estimated heat transfer in a closed air cavity bounded by ordinary materials e = 0.9 (Bekkouche et al., 2013)

By directly implementing LBNL THERM 7.4 into the design tool through the Grasshopper plugin Ladybug (Roudsari & Pak, 2013), the thermal performance of the cellular structure is analysed by performing heat flux simulations of horizontal cross-sections of the geometry. The calculations are based on two-dimensional simulations, where three types of heat transfer are included. Conduction and radiation are both modelled explicitly with the Finite Element Method (FEM) and a view-factor calculation, whereas convection is estimated through correlations and heat transfer coefficients (Huizenga et al., 1999). Three-dimensional heat transfer is not taken into account, assuming that the main heat flow is directed horizontally due to the temperature differences between indoors and outdoors. Furthermore, the influence of buoyancy driven natural convection within the closed cells is simplified by using film coefficients and neglecting the cell height. By using this simplified, automated, integral simulation process, the thermal performance of each layer can be assessed to derive a mean U-value for the whole element.
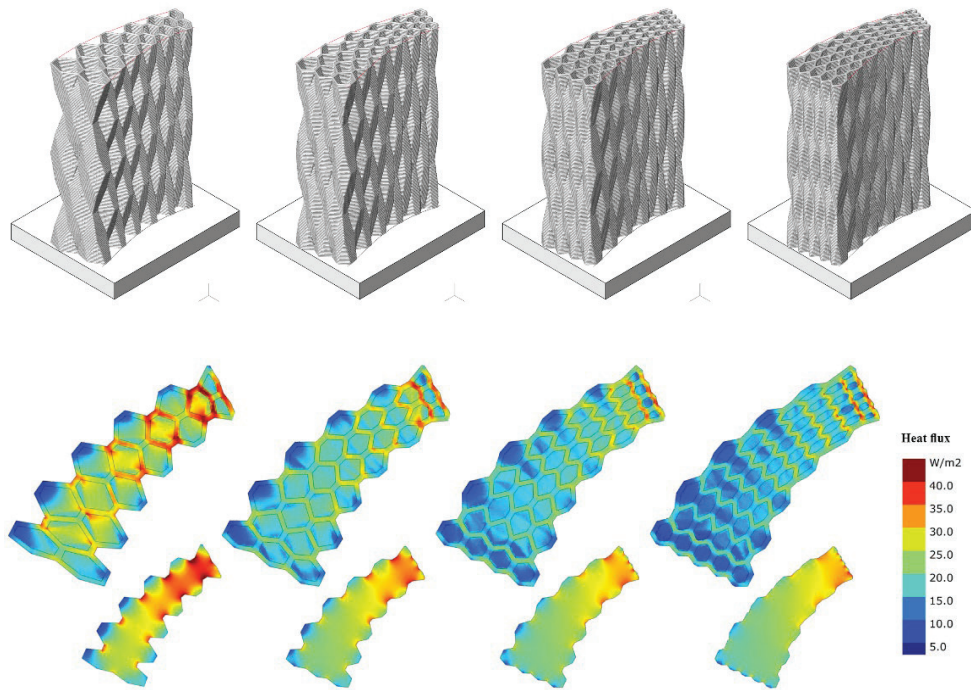
FIG. 8 Design variations of a wall element with increasing cell count in y-direction; visualisation of simulated heat flux for one exemplary layer each with and without internal cellular structure (Jaugstetter, 2020; adapted by David Briels).

TABLE 1 Geometrical properties of design variations of a wall element, as shown in Fig. 8, and results for thermal assessment.

CELL COUNT (Y)	1 / 2	2 / 3	3 / 4	4 / 5
Max cell size (y)	199 mm	129 mm	87 mm	65 mm
Wall thickness	150 – 450 mm	190 – 460 mm	220 – 460 mm	230 – 460 mm
air/solid-ratio	1,54	1,36	1,11	0,86
U-Value$_{tot}$ (cell)	0,71 W/m^{2}K	0,63 W/m^{2}K	0,61 W/m^{2}K	0,57 W/m^{2}K
U-Value$_{proj}$ (cell)	1,07 W/m^{2}K	0,80 W/m^{2}K	0,71 W/m^{2}K	0,64 W/m^{2}K
U-Value$_{proj}$ (solid)	1,28 W/m^{2}K	1,11 W/m^{2}K	1,05 W/m^{2}K	1,01 W/m^{2}K

A study of four design variations (see Fig. 8) uses a decreasing cell size from 200 to 65 mm and a cell count increasing from two to five. The thermal performance is visualised by a simulated heat flux and quantified by calculated U-values for one exemplary layer respectively. The areas with a heat flux of 25 W/m^2 or higher (yellowish to red) are visibly reduced, decreasing the calculated U-Value$_{tot}$ (from 0.71 W/m^{2}K to 0.57 W/m^{2}K (see Table 1). Due to higher geometrical resolution, the size of cells and thickness variation is reduced, while the amount of surface undulations and the size of the heat transferring surface is increased. This is indicated by an increase of the minimum wall thickness from 150 to 230 mm (see Table 1) and boundary line length in cross-sections, which are used for the calculation of the U-Value$_{tot}$. Projecting the boundary line on the guide surface results in a U-Value$_{proj}$ for the heat transfer through the wall element, allowing an improved comparability between variants. Comparing the calculated U-Value$_{proj}$ (cell) of the elements with cellular structure to the same geometries without air cavities (solid) a thermal enhancement of 16 to 37 % is evidenced for these four design variations. The increased thermal performance of the design variations can partially be attributed to the internal cellular structure, specifically to the reduced cell size resulting in lower convective heat transfer and the wall geometry resulting from the arrangement of cells.

At the same time, the air to solid ratio is decreasing, which implies an increase in heat conduction through solids, though the tipping point for the total heat transfer seems to not yet have been reached (compare Fig. 7).

3.3.2 Printability

The main constraint on 3DCP remains its buildability, specifically of free-standing and unsupported complex geometries requiring the concrete filament to cantilever. Cantilevering geometries can be categorised in terms of local and global inclinations, where local inclination is the result of cantilevering parts of the undistorted, often internal, geometry. Global inclination is the cantilevering geometry resultant of distortion of the overall geometrical design. The overhang is then defined as the eccentricity of the filament compared to the underlying layer, by calculating the projected distance between the two print paths. Short path segments are expected to be less critical despite having large overhangs; to account for this a segment length threshold is introduced with a value equal to the filament width.

The factor of time plays a large role for 3DCP, as viscosity increases over time to a degree where it can no longer be extruded (Buswell, Leal de Silva, Jones, & Dirrenberger, 2018). This is reflected in the design and print path generation as layer cycle time, with a lower limit being the buildability and the upper limit being defined by the bond strength between layers. To maintain geometric freedom and ensure manufacturability the path length is allowed to deviate in accordance with these limits, while the tool velocity is kept constant.

An estimated print duration is calculated based on the total print path length, where a correction factor based on directional changes is introduced to account for inevitable acceleration and deceleration of the robot (see Equation 3).

$$t_{layer} = \frac{l}{v_{robot}} + f \qquad\qquad (3)$$

3.4 PARTITIONING

The layer cycle time significantly influences the concrete extrusion process, with layer adhesion deteriorating for longer print paths (Wangler et al., 2016). No matter whether the elements are prefabricated or printed in-situ, their size is limited as a result of layer adhesion. For off-site printed elements, the size of these elements is additionally limited by transportation. Hence, a geometrical joint following the logic of the cellular structure is conceptualised, creating an interlocking connection between multiple elements. The convex and concave areas of the cells form either female or male joints, expected to be beneficial for force transmission and minimising thermal loss. To ensure the precise fit of the joint, shrinkage and interpolated print path geometry need to be controlled. In this research, joints are designed with tolerance on the print path to compensate for the discrepancy between the digital and real geometry. A wall design of two elements with their joint solution is shown in Fig. 9.
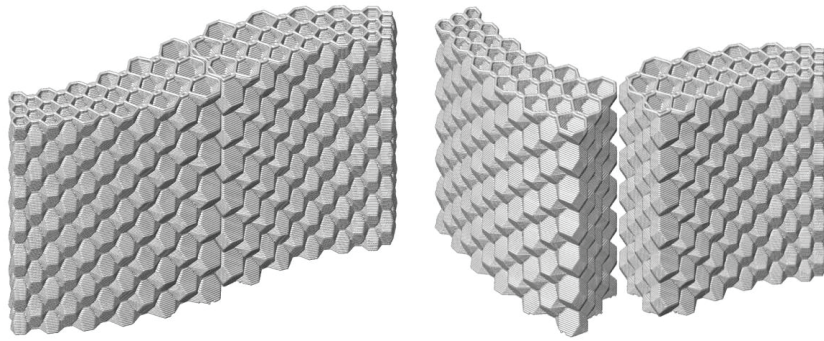
FIG. 9 Wall design composed of two elements joined together with cell-like joints (Jaugstetter, 2020)

4 EXPERIMENTAL RESULTS AND VALIDATION

4.1 MANUFACTURING PROCEDURE

For the placement of concrete filament, a KUKA KR150 L110 6-axis robot provided by the Chair of Building Realisation and Robotics at the Technical University of Munich has been used. The robot can reach a distance of 3500 mm with a maximum payload of 110 kg at the end effector and is mounted on a 7 m rail, which is implemented as a linear 7th axis. The robot was equipped with a custom end-effector, which includes a quick-change system for interchanging nozzles (Henke et al., 2018). Since live communication between design environment and robot was not possible due to the architecture of the controller, a translation was made from the print path to machine instructions with the Grasshopper plugin KUKA-PRC (Association for Robots in Architecture, 2020). The material that was used for the demonstrator objects is a lightweight aggregate concrete, using cement, water, and expanded glass granulate (Matthäus et al., 2020), resulting in a low density concrete of 300 – 800 kg/m^3 that has a relatively high pressure resistance of 1.4 – 1.8 N/mm^2. The concrete was batch-fed to a Knauf PFT Swing L FC-400V concrete pump with a feed-rate of 3.5-10.0 l/min, conveying the material through a 10-metre hose with 25 millimetre diameter.
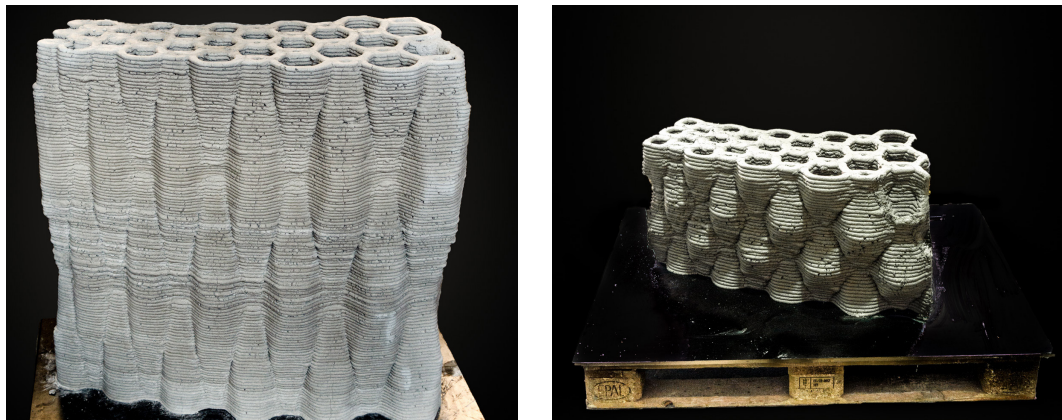

FIG. 10 3D printed demonstrator A with cell height of 740 mm (left) and demonstrator B with cell height 370 mm (right) (Jaugstetter, 2020)

Two demonstrator objects have been printed with the cellular geometry to validate the design tool for printability. These demonstrator objects will be referred to as 'A' and 'B', both designed to fit on a single pallet with dimensions of 1200 x 800 mm for ease of transportation (see Fig. 10). Demonstrator A has a cell height of 740 mm as defined by a maximum overhang of 4 mm, demonstrator B has a reduced cell height of 370 mm with 6.2 mm as maximum overhang to assess the stability of the cellular structure (see Table 1 for main characteristics of the designed demonstrator objects). For the demonstrator objects a nozzle of 22 mm diameter was used, which caused clearly visible filaments but removed the need for orienting the nozzle tangential to the printing path (Henke et al., 2020).

TABLE 2 Summary of characteristics of demonstrator objects in design phase (Jaugstetter, 2020)

	DEMONSTRATOR A	DEMONSTRATOR B
Base dimensions	1200 x 800 mm	1200 x 800 mm
Element height	1040 mm	1040 mm
Layers	116 layers at 9 mm	116 layers at 9 mm
Cell height	740 mm	244 mm
Maximum overhang per layer	4.1 mm	6.2 mm
Thickness	240 – 450 mm	240 – 450 mm
Cell diameter	340 – 870 mm	340 – 870 mm
Total print path length	1666.4 m	1666.2 m
Estimated weight	427 kg	427 kg

4.2   PRINTABILITY

To ensure bonding of the print path within a horizontal layer, an alteration to the digital geometry was made by partially overlapping the path. For a filament width of 22 mm, a distance between the centreline of two paths of 5 mm has been observed to ensure appropriate bonding between horizontal extrusions. Secondly, a layer cycle time correction factor has been derived from predicted times and cycle times as measured during the manufacturing process. With a correction factor of f_{robot} = 0.033 [s/°] an average deviation of 1.3 % between predicted and measured cycle time was be calculated (see Table 2).

TABLE 3 Comparison of predicted and measured layer cycle times (Jaugstetter, 2020)

LAYER	PREDICTED CYCLE TIME (S)	MEASURED CYCLE TIME (S)	DEVIATION
5	59.9 s	62 s	3.4 %
35	65.5 s	64 s	2.3 %
50	69.1 s	70 s	1.3 %
7-81	Ø 70.4 s	Ø 71.3 s	Ø 1.3 %

5   CONCLUSION

5.1   DESIGN TOOL AND FABRICATION

This research has shown the extrusion-based additive manufacturing with lightweight concrete to be capable of creating structures with enclosed cells. With the implementation of such cellular structures to a wall geometry, functionally enhancing the material for improved thermal performance has been achieved. Combined with a new design language, this customised geometry for a mono-material building component can thus represent a viable alternative to the conventional multi-material layered constructions.

However, limitations are still present with the lightweight concrete extrusion in a matter of achievable cell sizes and design freedom. The collapse of the outermost cells of the second demonstrator object has suggested that neighbouring cells can structurally support each other, allowing for steeper overhangs to be created inside than at the border (Bos et al., 2016).

The integration of fabrication constraints into a fabrication-aware design tool provides a possible solution for creating complex geometries customised for the manufacturing method, e.g., ensuring print path continuity across layers without compromising build time by preventing manufacturing interruptions. Print path continuity for manufacturing in construction may become obsolete with advances in the field, though in terms of build time it will likely remain advantageous as retractions and travel are not required (Jin, He, Fu, Gan, & Lin, 2014).

The implementation of a prognosis on manufacturing data in the design tool provides direct feedback to the user for refinement of the design in terms of resulting printability, material cost, and time. This integration allows for the creation of complex geometry with increased ease of use, allowing for more designers to interact with the digital manufacturing technology in construction. In turn, this could improve the distribution of digital concrete manufacturing, as currently a lack of experts in the field of complex design and machinery limits the adoptability (Buswell et al., 2018).

5.2   THERMAL PERFORMANCE

An ideal air layer thickness for the reduction of heat flux in a cavity wall was determined by Bekkouche et al. (2013), as between 40 and 60 mm, and, according to Gibson et al. (2014), at a cell size of 10 mm or lower, convection within closed cells can be neglected. Concrete extrusion with filament widths of around 20 mm limit the possibilities to create foam-like cellular structures without a decrease of the air to solid ratio, in which density causes the filament to act as a thermal bridge. This proportion is currently restricted by the low print resolution of the manufacturing process. This print resolution cannot be increased as smaller filament widths would substantially slow down the build rate, inhibiting either the printability or buildability of the material. In addition, the arrangement of the cells and the resulting wall geometry, as well as surface area, influence the thermal behaviour.

By using the integrated workflow for performance feedback within the design process, the thermal performance can be optimised. In the example case of four design variations (see Fig. 8) the reduction of cell size (in y direction) from 199 mm to 65 mm led to a substantial improvement of the U-Value$_{proj}$ by 40 % even though the air to solid ratio dropped from 1.54 to 0.86. Comparing the elements with cellular structure to the same geometries without air cavities a thermal enhancement

of 16 to 37 % is evidenced for these four design variations. This is based on a two-dimensional representation of the cellular geometry, where conduction and radiation are explicitly modelled in a finite element model and with a view-factor calculation whereas convective heat transfer is calculated based on heat transfer coefficients (Huizenga et al., 1999). Irregularities as a result of meshing of several complex layers have been seen to lead to anomalies in the simulation results, reducing the total number of useable thermally assessed layers. No measurements were taken from the manufactured demonstrators, while only scarce literature of digital manufactured concrete elements tested for thermal conductivity exists.

5.3   OUTLOOK

With the further development of 3DCP technology with the goal of achieving higher resolution and advances in eccentrically layering of filament, more complex geometries with smaller air cavities could be designed and manufactured that allow for further improvement in thermal performance. By now the estimated U-Value$_{proj}$ of the design variations up to 0.64 W/m2K still does not reach the common standard values for external walls, for example compared to the reference value of 0.28 W/m^{2}K in the German Energy Conservation Regulation (*EnEV*, 2007). However, this paper shows that with further improvements it seems feasible to thermally enhance mono-material lightweight concrete wall elements by adding and optimising an internal cellular structure to fulfil these requirements. To ensure buildability, the design tool could be extended to contain advanced structural feedback, preventing the element from collapse during the manufacturing process.

The thermal heat flux simulations should be extended by simulating the three-dimensional heat flow through the element and especially checking the influence of the buoyancy-driven natural convection within the closed cells. The theoretical assessment of the thermal performance via simulations should be tested and validated through heat flux measurements on the prototypes. In addition, filled cell geometries with porous materials could be simulated and researched in terms of their thermal behaviour as an application for particle bed processes, which provide higher print resolutions and thus the possibility to create more foam-like cellular structures.

References

Agustí-Juan, I., & Habert, G. (2017). Environmental design guidelines for digital fabrication. *Journal of Cleaner Production*, *142*, 2780–2791. https://doi.org/10.1016/j.jclepro.2016.10.190

Association for Robots in Architecture. (2020). *KUKA|prc*. https://www.robotsinarchitecture.org/kukaprc

Bankvall, C. (1972). *Natural convective heat transfer in insulated structures*. https://portal.research.lu.se/ws/files/4596708/8227870.pdf

Bekkouche, S. M.A., Cherier M. K., Hamdani, M., Benamrane, N., Benouaz, T., & Yaiche, M. R. (2013). Thermal resistances of air in cavity walls and their effect upon the thermal insulation performance. *International Journal of Energy and Environment*, *4*(3), 459–466. http://www.ijee.ieefoundation.org/vol4/issue3/IJEE_11_v4n3.pdf

Bos, F., Wolfs, R., Ahmed, Z., & Salet, T. (2016). Additive manufacturing of concrete in construction: potentials and challenges of 3D concrete printing. *Virtual and Physical Prototyping*, *11*(3), 209–225. https://doi.org/10.1080/17452759.2016.1209867

Bos, F., Wolfs, R., Ahmed, Z., & Salet, T. (2019). Large scale testing of digitally fabricated concrete (DFC) elements. In *RILEM Bookseries* (Vol. 19, pp. 129–147). Springer Netherlands. https://doi.org/10.1007/978-3-319-99519-9_12

Buswell, R. A., Leal de Silva, W. R., Jones, S. Z., & Dirrenberger, J. (2018). 3D printing using concrete extrusion: A roadmap for research. In *Cement and Concrete Research* (Vol. 112, pp. 37–49). Elsevier Ltd. https://doi.org/10.1016/j.cemconres.2018.05.006

Dubai Future Foundation. (n.d.). *Office of the Future*. Retrieved September 4, 2020, from https://www.dubaifuture.gov.ae/our-initiatives/office-of-the-future/

EnEV. (2007). https://www.gesetze-im-internet.de/enev_2007/BJNR151900007.html

Falliano, D., Crupi, G., De Domenico, D., Ricciardi, G., Restuccia, L., Ferro, G., & Gugliandolo, E. (2020). Investigation on the Rheological Behavior of Lightweight Foamed Concrete for 3D Printing Applications. In *RILEM Bookseries* (Vol. 28, pp. 246–254). Springer. https://doi.org/10.1007/978-3-030-49916-7_25

Furet, B., Poullain, P., & Garnier, S. (2019). 3D printing for construction based on a complex wall of polymer-foam and concrete. In *Additive Manufacturing* (Vol. 28, pp. 58–64). Elsevier B.V. https://doi.org/10.1016/j.addma.2019.04.002

Gibson, L. J., & Ashby, M. F. (2014). Thermal, electrical and acoustic properties of foams. In *Cellular Solids: Structure and Properties, Second Edition* (pp. 283–308). Cambridge University Press. https://doi.org/10.1017/CBO9781139878326

Goldman, R., Schaefer, S., & Ju, T. (2004). Turtle geometry in computer graphics and computer-aided design. *CAD Computer Aided Design*, *36*(14), 1471–1482. https://doi.org/10.1016/j.cad.2003.10.005

Henke, K., Talke, D., & Matthäus, C. (2020). *Additive Manufacturing by Extrusion of Lightweight Concrete - Strand Geometry, Nozzle Design and Layer Layout* (pp. 906–915). https://doi.org/10.1007/978-3-030-49916-7_88

Huizenga, C., Arasteh, D., Finlayson, E., Mitchell, R., Griffith, B., & Curcija, D. (1999). *THERM 2.0: a building component model for steady-state two-dimensional heat transfer*. https://escholarship.org/uc/item/66n7n302

Jaugstetter, F. (2020). *Design Tool for Extrusion Based Additive Manufacturing of Functionally Enhanced Lightweight Concrete Wall Elements with Internal Cellular Structures*. Technische Universität München.

Jin, Y. an, He, Y., Fu, J. zhong, Gan, W. feng, & Lin, Z. wei. (2014). Optimization of tool-path generation for material extrusion-based additive manufacturing technology. *Additive Manufacturing*, *1*, 32–47. https://doi.org/10.1016/j.addma.2014.08.004

Keating, S. J., Leland, J. C., Cai, L., & Oxman, N. (2017). Toward site-specific and self-sufficient robotic fabrication on architectural scales. *Science Robotics*, *2*(5). https://doi.org/10.1126/scirobotics.aam8986

Markin, V., Ivanova, I., Fataei, S., Reißig, S., & Mechtcherine, V. (2020). Investigation on Structural Build-Up of 3D Printable Foam Concrete. In *RILEM Bookseries* (Vol. 28, pp. 301–311). Springer. https://doi.org/10.1007/978-3-030-49916-7_31

Matthäus, C., Back, D., Weger, D., Kränkel, T., Scheydt, J., & Gehlen, C. (2020). *Effect of Cement Type and Limestone Powder Content on Extrudability of Lightweight Concrete* (pp. 312–322). https://doi.org/10.1007/978-3-030-49916-7_32

McNeel & Associates. (n.d.). *Rhinonoceros (Rhino) Version 6.0*. Retrieved September 4, 2020, from https://www.rhino3d.com/

Roudsari, M. S., & Pak, M. (2013). *LADYBUG: A PARAMETRIC ENVIRONMENTAL PLUGIN FOR GRASSHOPPER TO HELP DESIGNERS CREATE AN ENVIRONMENTALLY-CONSCIOUS DESIGN*.

Van Der Putten, J., Van Olmen, A., Aerts, M., Ascione, E., Beneens, J., Blaakmeer, J., De Schutter, G., & Van Tittelboom, K. (2020). 3D Concrete Printing on Site: A Novel Way of Building Houses? In *RILEM Bookseries* (Vol. 28, pp. 712–719). Springer. https://doi.org/10.1007/978-3-030-49916-7_71

Vantyghem, G., Steeman, M., De Corte, W., & Boel, V. (2017). Design of cellular materials and meso-structures with improved structural and thermal performances. *Proceedings of the 12th World Congress of Structural and Multidisciplinary Optimisation*. http://hdl.handle.net/1854/LU-8524436

Vantyghem, G., Steeman, M., De Corte, W., & Boel, V. (2020). Design Optimization for 3D Concrete Printing: Improving Structural and Thermal Performances. In *RILEM Bookseries* (Vol. 28, pp. 720–727). Springer. https://doi.org/10.1007/978-3-030-49916-7_72

Wangler, T., Lloret, E., Reiter, L., Hack, N., Gramazio, F., Kohler, M., Bernhard, M., Dillenburger, B., Buchli, J., Roussel, N., & Flatt, R. (2016). Digital Concrete: Opportunities and Challenges. *RILEM Technical Letters*, *1*, 67. https://doi.org/10.21809/rilemtechlett.2016.16

Weger, D., Kim, H., Talke, D., Henke, K., Kränkel, T., & Gehlen, C. (2020). *Lightweight Concrete 3D Printing by Selective Cement Activation – Investigation of Thermal Conductivity, Strength and Water Distribution* (pp. 162–171). https://doi.org/10.1007/978-3-030-49916-7_17